Limitations of traditional models for perfusion

Constantin Sandmann, Erik A. Hanson, Alexander Malyshev, Arvid Lundervold, Jan Modersitzki, Erlend Hodneland

***Abstract*—In perfusion imaging the usage of traditional one-compartment models to estimate hemodynamic parameters like blood flow (perfusion), blood volume and mean transit times is widespread. In this paper we show limits of traditional models to recover perfusion. We derive the theoretical details related to voxel wise perfusion estimation when the image resolution reach the spatial scale of the capillary systems. Based on modeling of porous media flow, we introduce a continuous model for propagation of a tracer in the capillary tissue. We show that the proposed model can be understood as a coupled set of traditional one-compartment models. It is furthermore demonstrated that traditional models (deconvolution, maximum slope) are accurately recovering the perfusion if applied to the entire domain. However, we also show both analytically and experimentally that results of traditional models are not meaningful if applied only to smaller portions of the system, and will result in over estimation of perfusion. Evidence of real patient data is provided, indicating that this effect might also be observed on coarse scale in real-life applications.**

I. Introduction

Quantitative measurements of hemodynamic medical parameters based on tracer kinetic modeling are widespread both in research and in clinical practice [1], [2], [3]. In the present work, we focus on mathematical models to estimate blood perfusion (cerebral blood flow, CBF), blood volume (cerebral blood volume, CBV), and mean transit time (MTT) of the brain from dynamic image data using tracers.

While hardware limitations in medical imaging for decades have confined studies to only handle larger tissue regions or full organs, modern imaging technology and voxel based analysis give rise to aspirations about detailed perfusion maps with sub-millimeter precision. Examples of estimated parameter maps can be found in [2], [3]. We expect the development to continue and that imaging systems will reach a resolution where a single capillary system spans over several voxels. Quantitative perfusion maps, as well as other parameter maps arising from tracer kinetic modeling, can be combined with anatomical information, and the maps have proven to be of particular value in e.g. stroke studies for localization of trauma. Among the physiological parameters obtainable from tracer kinetic models, CBF has found particularly difficult to describe reliably on a voxel-basis [4]. These limitations in perfusion estimations are caused by issues in the numerical implementation [4], but might also depend on over-simplified dynamic models, which were originally designed to describe larger volumes of interest [5].

There have been several approaches to clarify the concept of perfusion in a continuous sense, which perviously has been suffering from lack of precise mathematical definitions coinciding with the common understanding of perfusion as the delivery of arterial blood to the capillary system. In [7], the problem of scale dependent continuous perfusion was discussed. Perfusion defined as flow entering a voxel will scale with voxel size, and this notion of perfusion is therefore unsuited. More recently a two-compartment model was introduced as a precise definition of local perfusion [8]. However, clinical evaluation of the proposed modeling is still pending.

In this work we focus on the validity of traditional perfusion models. We do this by simulating a tissue patch with one inlet, one outlet, and a capillary system in between. A directional flow field for the patch is set up according to Darcy's law from porous media flow [9]. After that, contrast agent propagation in this patch is simulated using standard transport equations. We show that the discretized 3D system can be equivalently described by a coupled set of multiple traditional one-compartment models, in line with the physical environment where each control volume is feeding their direct neighbors.

We then proceed to demonstrate that traditional models like deconvolution or the maximum slope model are able to recover the perfusion accurately if applied to the entire domain fed by the incoming flow. However, when applying the traditional models to isolated parts of the full system, we find that local perfusion in coupled systems is not straightforward to define. In order to cope with this issue, two possible definitions of voxel-wise perfusion are presented: A definition P_{v} describing the local inflow into a voxel, but otherwise not fulfilling the traditional concept of perfusion, and then a tailored definition of perfusion P_{s} for continuous models.

Our results show that perfusion results from traditional models tend to overestimate P_{s} and to underestimate P_{v} if they are applied only to parts of the full system. Analytic results are given, which show that the recovered perfusion depends on all upstream flow and not only on the local value. We also show results indicating that overestimation of perfusion due to coupling might also be found in real data.

II. Traditional Models for perfusion

In this section we describe the convolution- and the maximum slope model, two widely used one-compartment pharmacokinetic models for measurements of CBF and CBV [2], [3], [4]. For the remaining, they are referred to as *traditional* models.

Let Ω_i be an arbitrary control volume with one inlet and one outlet, and let $C(t)$ denote the average contrast agent (CA) concentration within Ω_i at timepoint t. The traditional models assume that the change of concentration at timepoint t can be described by the ordinary differential equation

$$C'(t) = P_{\mathrm{a}} c_{\mathrm{a}}(t) - P_{\mathrm{v}} c_{\mathrm{v}}(t), \quad C(0) = 0. \tag{1}$$

Here $c_{\mathrm{a}}, c_{\mathrm{v}}$ are the CA plasma concentrations at the inlet and outlet of Ω_i, and $P_{\mathrm{a}}, P_{\mathrm{v}}$ are the corresponding perfusion values at these locations. In the following it is assumed that the plasma tracer concentration c_{a} at the inlet is known. In clinical practice this can be accounted for by measuring c_{a} in a feeding artery [10]. Since c_{v} is usually unknown, additional assumptions need to be made if one wants to reconstruct P_{a} from a given tissue curve C. The convolution model and the maximum slope (MS) model diverge in further assumptions.

A. The Convolution Model

For the deconvolution model, one approach is to assume there is an unknown probability distribution of transit times h through Ω_i, cf. [1]. This leads to

$$P_{\mathrm{v}}c_{\mathrm{v}}(t) = P_{\mathrm{a}}(h * c_{\mathrm{a}})(t) := P_{\mathrm{a}} \int_0^t c_{\mathrm{a}}(s)h(t-s)\,\mathrm{d}s. \quad (2)$$

Combining this with (1) yields $C'(t) = P_{\mathrm{a}}c_{\mathrm{a}}(t) - P_{\mathrm{a}}(h * c_{\mathrm{a}})(t)$. Integrating this equation and using basic properties of the convolution one obtains the general solution

$$C(t) = (I * c_{\mathrm{a}})(t). \quad (3)$$

where the *impuls-response function* I is defined as $I(t) := P_{\mathrm{a}}(1 - \int_0^t h(s)\,\mathrm{d}s)$. The task of identifying $I(t)$ given a tissue curve $C(t)$ and an arterial input function $c_{\mathrm{a}}(t)$ is a deconvolution problem. If $I(t)$ is recovered, P_{a} can subsequently be estimated as $P_{\mathrm{a}} = \max_t I(t)$. There are several methods to perform the deconvolution. A standard approach using Fourier-based algorithms is sensitive to the presence of noise [10]. Another class of deconvolution algorithms gaining increasing attention are based on Bayesian modeling [11]. However the numerical handling is still difficult since complex and error-prone numerical integration has to be performed [11]. A popular class among deconvolution algorithms is based on singular value decomposition (SVD) [10]. These algorithms have shown to be robust for a reasonable noise level. Also, they can be easily adapted to be robust against delays in tracer arrival using block-circular structures (bSVD cf. [12]). In order to identify the impuls-response function $I(t)$ from simulated data, we hence decided to use the bSVD model as proposed in [12].

B. The Maximum Slope Model

In the MS model it is assumed that when c_{a} has its maximum, only a negligible amount of CA is leaving the system [13]. For this time interval, (1) reduces to

$$C'(t) = P_{\mathrm{a}}c_{\mathrm{a}}(t), \quad C(0) = 0. \quad (4)$$

One can see that if c_{a} has a maximum, also C' must have a maximum since stationarity in P_{a} is assumed. Hence, it holds that

$$P_{\mathrm{a}} = \frac{\max_t C'(t)}{\max_t c_{\mathrm{a}}(t)}. \quad (5)$$

III. A Synthetic Model for Capillary Flow

The validity of the traditional methods rely on a ROI with only one inlet and one outlet, and for the convolution model that transition times are prescribed by some probability distribution. In fact, the assumption of one inlet and one outlet may easily be violated when we locally describe CA propagation through a larger volume with a highly developed capillary system. For this type of model system we instead expect a set of coupled transport equations where each voxel can be regarded as an inlet for surrounding voxels. Hence, in order to make a realistic synthetic model for capillary flow, we decided to describe the CA propagation as a spatially coupled transport process, i.e. using partial differential equations (PDE) for transport. This PDE model is used for validation of the traditional models.

Compatible with the assumption of stationary, incompressible flow at low Reynold numbers within the capillary system [14], we will use Darcy's law to simulate capillary flow [9]. This is in agreement with previous work on capillary perfusion [15], [16].

A major difference between our coupled flow model and traditional tracer kinetic modeling is the normalization of the flow field. In traditional models normalization is performed with respect to the volume and leads to the units of perfusion [mm^3/s/mm^3], cf. [1]. To avoid a discretization dependent flow field for the PDE model, we instead use vector valued surface fluid flux $q = q(x)$ with units [mm^3/s/mm^2] as the fluid carrying parameter, in agreement with geoscience and porous media simulation theory. The fluid flux is a vector field describing the volume of fluid per unit time flowing across a sliced unit area of the sample. Apart from the normalization with respect to surface, the assumptions of linearity and stationarity in the fluid flux are in complete agreement with standard pharmacokinetic modeling [1].

A. Modelling Capillary Blood Flow

For the time being we will not consider contrast agent concentrations, but only the fluid flow in general. The fluid density is denoted by $\rho = \rho(x,t)$. The flux q as well as the porosity ϕ are assumed to be stationary and hence independent of time. Fluid entering and leaving the system is described by a source- and sink term $\tilde{Q} = \tilde{Q}(x)$ [mg/s/mm^3]. The continuity equation assuring conservation of fluid mass states

$$\frac{\partial(\phi\rho)}{\partial t} + \nabla \cdot (\rho q) = \tilde{Q}. \quad (6)$$

Furthermore, assuming that the fluid flow is steady-state and that the density of blood ρ is constant in space, we obtain $\nabla \cdot q = \tilde{Q}/\rho$. In order to scale away the density ρ we define Q [mm^3/s/mm^3] having the relation $\tilde{Q} := Q\rho$, thus transforming the equation into

$$\nabla \cdot q = Q. \quad (7)$$

Here the right hand side is a volume flux, only non-zero within the source or the sink. Elsewhere, (7) is concurrent with divergence free flow of an incompressible fluid. Low velocity

fluid flux in porous media is usually described by Darcy's law. Neglecting gravitational forces leads to [9]

$$q = -\frac{\mathbf{k}}{\mu}\nabla p. \tag{8}$$

Here, $\mathbf{k} = \mathbf{k}(x)$ is a permeability tensor, $p = p(x)$ is the pressure, and $\mu = \mu(x)$ is the viscosity of the fluid. For simplicity, we will assume that $\mathbf{k}$ is a symmetric and positive definite tensor with only nonzero diagonal elements $\mathbf{k}_{ii} = k$, in accordance with a homogeneous porous medium. Equations (7) and (8) can be combined, yielding the following elliptic partial differential equation in the pressure field p within the closed domain Ω,

$$\left| \begin{aligned} \nabla \cdot \left(-\frac{\mathbf{k}}{\mu}\nabla p\right) &= Q, \qquad && x \in \Omega \\ n \cdot \nabla p &= 0, && x \in \partial\Omega. \end{aligned} \right| \tag{9}$$

For the outward unit normal $n = n(x)$, Neuman boundary conditions are reflecting zero fluid flux $q(x)$ across the boundary $\partial\Omega$. After solving (9) for the pressure p, the flux field can be estimated according to (8) from the obtained pressure map.

B. Modelling Indicator Dilution

The introduced framework in Section III-A does not relate flow to propagation of a contrast agent. This section describes a model for CA propagation in the tissue as it is homogeneously dissolved in the evolving fluid. We assume that the CA is entering the domain along with the fluid flowing in via the source, and similarly extracted at a sink. The resulting CA concentration map is a simulation of the CA concentrations observed within real MRI measurements.

In order to define meaningful and continuous contrast agent concentrations, we first describe CA concentration in an (arbitrarily) small tissue volume Ω_i. Let V_i be the volume of an arbitrary control region Ω_i and let v_i be the blood volume within Ω_i. The porosity $\phi_i := v_i/V_i$ reflects the relative space within the vascular system. We further introduce $C_i(t)$ and $c_i(t)$ as the CA concentration in Ω_i with respect to V_i and v_i respectively. By definition, we obtain the relation $C_i(t) = \phi_i c_i(t)$. The rate of change of tracer molecules within an arbitrary control volume Ω_i can hence he phrased as

$$\frac{\mathrm{d}}{\mathrm{d}t}\int_{\Omega_i} C_i(t)\,\mathrm{d}x = \int_{\Omega_i}\frac{\mathrm{d}}{\mathrm{d}t}(\phi_i c_i(t))\,\mathrm{d}x = \int_{\Omega_i}\phi_i\frac{dc_i}{dt}\,\mathrm{d}x, \tag{10}$$

where the assumption of stationary ϕ_i was used. Since we expect mainly transport and marginal diffusion, the change in tracer mass within Ω_i occurs from advective flow and the source and sink field Q. Let us write the source- and the sink term as $Q = Q_{\mathrm{si}} + Q_{\mathrm{so}}$ where $Q_{\mathrm{si}} < 0$ is the sink and $Q_{\mathrm{so}} > 0$ is the source, and zero elsewhere. Note that $\int_\Omega Q\,\mathrm{d}x = 0$. The change in contrast agent at time point t from fluid entering the control volume can be written as

$$-\int_{\partial\Omega_i} c_i(t)(q_i\cdot n)\,\mathrm{d}s + \int_{\Omega_i} c_{\mathrm{a}}(t)Q_{so,i}\,\mathrm{d}x + \int_{\Omega_i} c_i(t)Q_{si,i}\,\mathrm{d}x, \tag{11}$$

where n is the outward unit normal on $\partial\Omega_i$. In standard pharmacokinetic modeling, c_{a} is referred to as the arterial input function (AIF). From the principle of conservation of tracer molecules, (10) and (11) must balance for each control volume Ω_i, such that

$$\begin{aligned} &\int_{\Omega_i}\phi_i\frac{dc_i}{dt}\,\mathrm{d}x + \int_{\partial\Omega_i} c_i(t)(q_i\cdot n)\,\mathrm{d}s \\ &= \int_{\Omega_i} c_{\mathrm{a}}(t)Q_{so,i}\,\mathrm{d}x + \int_{\Omega_i} c_i(t)Q_{si,i}\,\mathrm{d}x. \end{aligned} \tag{12}$$

Now, let the contrast agent concentrations, porosity, volume fluxes, and surface flux be continuous functions of space and time. Equation (12) is then consistent with the continuity equation on local form

$$\left| \begin{aligned} \phi\frac{\partial c}{\partial t} + \nabla\cdot(cq) &= c_{\mathrm{a}}Q_{\mathrm{so}} + cQ_{\mathrm{si}} && x\in\Omega,\ t>0, \\ c(x,t) &= 0 && x\in\Omega,\ t=0. \end{aligned} \right| \tag{13}$$

where we also added the initial condition $c(x,0) = 0$ in line with the physical problem of no tracer at $t = 0$. Equation (13) is a linear transport equation in $c(x,t)$. Following [17], (13) admits a unique local solution.

C. Relating the transport equation model with the traditional deconvolution model for perfusion

In this section we describe how the continuous model is related to the traditional deconvolution model. More specifically, we will show that in the continuous model, the flow into each voxel can be described by a traditional model with arterial input determined by adjacent upstream voxels.

Let us start by modeling the CA concentration in a given voxel Ω_i using traditional models. For sake of simplicity we assume that $Q_{\mathrm{so},i} = Q_{\mathrm{si},i} = 0$ within that voxel. Note that it is possible to extend the following approach also to voxels where this is not the case. Define the areas (voxel faces) of inflow and outflow over the boundary as $S_{\mathrm{in}} := \{x \in \partial\Omega_i : q_i(x)\cdot n(x) < 0\}$ and $S_{\mathrm{out}} := \{x\in\partial\Omega_i :\ q_i(x)\cdot n(x) > 0\}$ respectively. For the domain Ω_i we define the arterial input c_{in} as the weighted average of the tracer flux across S_{in}

$$c_{\mathrm{in}}(t) := \frac{\int_{S_{\mathrm{in}}} c(t)(q_i\cdot n)\,\mathrm{d}s}{\int_{S_{\mathrm{in}}} q_i\cdot n\,\mathrm{d}s}. \tag{14}$$

This allows us to define the perfusion P_{v} within Ω_i as the total fluid inflow divided by the volume,

$$P_{\mathrm{v}} := -\frac{1}{\mathrm{Vol}(\Omega_i)}\int_{S_{\mathrm{in}}} q_i\cdot n\,\mathrm{d}s. \tag{15}$$

Given an incompressible flow, let us now assume that the rate of fluid entering the region is the same as the rate of fluid leaving it. Then it holds that $P_{\mathrm{v}} = P_{\mathrm{out}}$ and we can describe c_i by the traditional model (1),

$$(\phi c_i)'(t) = P_{\mathrm{v}}(c_{\mathrm{in}}(t) - c_{\mathrm{out}}(t)). \tag{16}$$

Note that the upwind-discretization described in Section III-B models each voxel as a well-mixed compartment: it is assumed that the CA concentration at the outflow S_{out} equals the concentration within the voxel and that the concentration at the inflow is the concentration within the adjacent voxels. In

this case it follows that (16) reduces to $(\phi c_i)'(t) = P_{\mathrm{v}}(c_{\mathrm{in}}(t) - c_i(t))$ with solution

$$C_i(t) = \phi_i(J_i * c_{\mathrm{in}})(t) \text{ for } J_i(t) = (P_{\mathrm{in}}/\phi_i)e^{-(P_{\mathrm{v}}/\phi_i)t}. \quad (17)$$

The arterial input c_{in} is determined by (14), which recursively depends on all upstream voxels until the global arterial input is reached. To verify this relationship numerically, we simulated a tissue curve $C_i(t)$ using both the continuous PDE model as well as convolution in (17). We refer to the latter approach as *local convolution*. The two curves have an almost perfect match, as seen in Figure 1 (left).

As a direct consequence, it follows by recursion that for a given voxel at location i the concentration can be written as a convolution of the (global) arterial input function with the impulse response functions of all upstream voxels $\{1, \dots, l\}$, i.e.

$$C_n(t) = \Pi_{i=1}^{n}\phi_i \cdot ((J_1 * \cdots * J_n) * c_{\mathrm{a}})(t). \quad (18)$$

with the relation $J_i(s) := p_i \exp(-p_i(s))$ and $p_i = P_{\mathrm{v}}^i/\phi_i$. Following [18], the convolution of exponential functions with pairwise different parameters p_i is given by

$$(J_1 * \cdots * J_n)(s) = \sum_{i=1}^{n} \frac{\Pi_{j=1}^{n} p_j}{\Pi_{j=1, j\neq i}^{n}(p_j - p_i)} e^{-p_i s}. \quad (19)$$

See [18] for the case $p_i = p_j$ for some i, j. This relationship was also confirmed experimentally: Figure 1 (right) shows the impulse response function determined by (19) and the impulse response function obtained from deconvolving a tissue curve of the continuous model with the global arterial input function. The two curves coincide almost perfectly.

These results show that the PDE model and the convolution model are equal in terms of local, voxel wise flow estimates if the convolution model is applied with the correct, local arterial input. Also, the impulse response function obtained by convolution of the global arterial input function is identical to an analytical recursive convolution along all upstream voxels. This clearly demonstrates that the traditional models measure a non-local perfusion quantity along the streamlines, but only upstream, and the entire streamline length within the capillary system is not taken into consideration where the blood is providing the tissue with nutrients and oxygen. These results also support the idea presented in the next section that pointwise perfusion can be regarded a globally constant quantity along the streamlines, as it can only be estimated when the entire streamline characteristics are known.

D. Converting Flow to Perfusion

The model described in (9) uniquely determines the flux field $q(x)$. However, in pharmacokinetic modeling the parameter of interest is usually the CBF, which we will denote by $P(x)$ as the voxel wise field of perfusion. The surface flux and perfusion are physically distinct, and there are at least two differences between $q(x)$ and $P(x)$. First, the flux is a vector field and the perfusion is a scalar field. Second, the flux is normalized to a surface area and the perfusion is normalized to a volume. In the following we describe a method for converting flux into perfusion, motivated by our need to compare the PDE based ground-truth, vector valued flux field to the scalar valued perfusion field obtained by traditional methods.

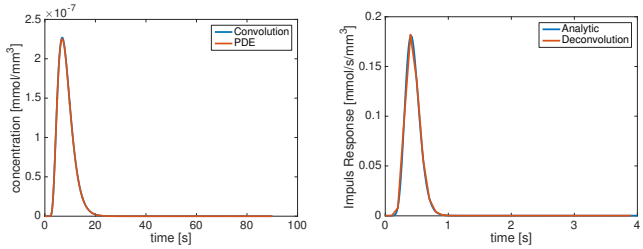

Figure 1. Left: Red curve shows the tissue curve of the continuous PDE model at location [32,35]. Blue curve shows simulation using (17) with experimental values of $P_{\mathrm{v}}^i = 5328$ ml/min/100ml and c_{in} taken locally from upstream voxels around the simulated voxel. The two curves have an almost perfect overlap. Note that the perfusion is unrealisticly high since normalization is performed with respect to the volume of only one voxel. Right: Red curve shows the computed impulse response functions at location [1,20] using the global arterial input function. Blue curve shows the analytic impulse response function given by (19). The two curves have an almost perfect overlap. These numerical experiments support the analytic considerations, that the computed impulse response function by traditional methods is not the directly feeding impulse response function, but rather a recursive impulse response function depending on all upstream voxels.

The common understanding of perfusion or volume flux $P(x)$ is the amount of blood feeding a tissue volume per unit time, with units [mm^3/s/mm^3]. One straightforward approach for converting flux into perfusion could be to estimate the perfusion as the total inflow (or outflow) of fluid (e.g. arterial blood) into a control region per unit time, and then normalizing with the control region volume. This is a valid approach only if the control regions are not feeding each other, and is therefore well-founded for the entire organ, in line with the theoretical foundation of traditional compartment models for perfusion where a control region has its own source of feeding arterial blood, independent of neighbor regions.

On the other hand, if the control region is a single voxel or a sub-division of an organ with sequentially feeding arterial blood, the traditional model assumptions are violated since every control region will feed its neighbours, thus becoming a coupled system of flow. Simply summing the total inflow into a voxel and dividing by the voxel volume will strongly overestimate the perfusion as the normalization refers to the wrong volume. This phenomenon is demonstrated in Figure 2 where the volume on the left has the true perfusion of $P_1 = F_0/(2V)$ for an incoming flow F_0 [mm^3/s] and distribution volume $2V$ [mm^3]. However, for another discretization as shown in the middle, the perfusion within each of these sub-volumes becomes $P_2 = F_0/V = 2P_1$. Taking the average across the two sub-volumes, it is clear that the perfusion is over-estimated with a factor of two. A discretization dependent perfusion estimate is not recommendable, and the perfusion estimate of P_2 is clearly wrong. This problematic issue was already identified by [7], stating that an incorrect normalization will lead to multiple counting of the same flow, and hence an overestimation of perfusion.

In the following we introduce a meaningful notion of perfusion for the continuous model. To do this, we will consider distribution volumes which are following the streamlines, as

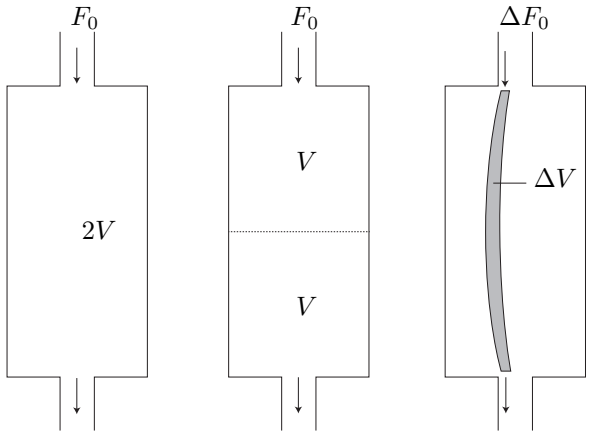

Figure 2. Perfusion within a small volume. Left: A compartment with volume $2V$ is exposed to a flow F_0 [mm^3/s] of fluid. By definition, the perfusion within this compartment becomes $P_1 = F_0/(2V)$. Middle: The same volume is divided into two compartments (e.g. voxels), and the perfusion for each of the compartments becomes $P_2 = F_0/V = 2P_1$. The discrepancy between the two discretizations occurs because the flow is counted twice as it is fed from one voxel to the other. Right: As a solution to the described problem we rather pick out a true distribution volume ΔV (area in this 2D sketch), which is a small area around a given streamline along the centre line of the grey area. This is the true distribution volume (area in this 2D sketch) which is fed with arterial blood from the incoming fractional flow ΔF_0. The correct perfusion within ΔV is therefore $\Delta F_0/\Delta V$. The entire compartment can further be divided into similar infinitesimal distribution volumes, thus providing locally correct perfusion estimates.

shown in Fig. 2 (right). For each point of a streamline we will select a small perpendicular disk with radius chosen in such a way that the total flow over each disk is constant along the streamline.

More precisely, let us consider an arbitrary streamline $S \subseteq \Omega \subseteq \mathbb{R}^3$ of length $l > 0$ and parametrization $s : [0, l] \to S$. We start by calculating the total flow over a small 2-D disc perpendicular to the streamline. Let $y \in S$ be an arbitrary location along the streamline. The total flow F over a 2-D disc $B(y, R(y))$ perpendicular to the flow field $q(y)$, centered at y and with radius $R : S \to \mathbb{R}^+$, is given by

$$F(y, R(y)) = \int_{B(y,R(y))} q(x) \cdot \nu \, \mathrm{d}x \text{ where } \nu := q(y)/|q(y)|. \tag{20}$$

In order to calculate the perfusion, we need to establish the volume of a small tube around the streamline. We will not consider a tube with constant radius, but one with spatially varying radii $r : [0, l] \to \mathbb{R}^+$. The total volume of such a tube surrounding the streamline is given by

$$V(r) = \int_0^l r(u)^2 \pi \, \mathrm{d}u. \tag{21}$$

Note that $R(y) := r(u)$ for some $u \in [0, l]$ satisfying $y = s(u)$. We define the perfusion at the arbitrary point y on the streamline as

$$P_\mathrm{s} := \lim_{\varepsilon \to 0} \frac{F(y, \varepsilon R(y))}{V(\varepsilon R(y))} \tag{22}$$

for $R(y) := 1/\sqrt{|q(y)|}$. Note that $F(y, \varepsilon r(u)) = F(y, \varepsilon R(y))$ and $V(\varepsilon r(u)) = V(\varepsilon R(y))$, and can be interchanged independent of parameterization. Also, the radii $R(y)$ are chosen in such a way that in the limit when $\varepsilon \to 0$, the perfusion is constant along the streamline. To see this, let us assume that q is differentiable with Jacobian J. Using a Taylor expansion of $q(x)$ around y, the Lagrange remainder theorem, as well as a change of coordinates $z = (x - y)/(\varepsilon R)$ yields

$$\begin{aligned} F(y, \varepsilon R(y)) &= \int_{B(y,\varepsilon R(y))} \nu^\top q(x) \, \mathrm{d}x \\ &= \int_{B(y,\varepsilon R(y))} \nu^\top q(y) + \nu^\top J(\xi)(x - y) \, \mathrm{d}x \\ &= \varepsilon^2 \pi + \int_{B(0,1)} \nu^\top J(\zeta) z (\varepsilon R(y))^3 \, \mathrm{d}z \\ &= \varepsilon^2 \left(\pi + \varepsilon \int_{B(0,1)} \nu^\top J(\zeta) z R(y)^3 \, \mathrm{d}z \right) \end{aligned}$$

$$F(y, \varepsilon R(y)) = \varepsilon^2 \Big(\pi + \varepsilon \int_{B(0,1)} \nu^\top J(\zeta) z R(y)^3 \, \mathrm{d}z \Big) \tag{23}$$

where $\zeta \in (0, z)$ and simplifications are due to $R(y) = 1/\sqrt{|q(y)|}$ and $\nu := q(y)/|q(y)|$. It follows from (22) that

$$P_\mathrm{s} = \left(\int_0^l r(u)^2 \, \mathrm{d}u \right)^{-1} \tag{24}$$

where we changed to the parameterized version of $V(r)$. Equation (24) is independent of the spatial location y along the streamline and an explicit formula for converting flux into perfusion, showing that the perfusion scales with the streamline length l, as well as with the geometry of the domain, represented by the radii $r(u)$.

E. A Method to Estimate local Porosity

It is known from literature on traditional models for perfusion that CBV for the entire compartment can be expressed as

$$\phi = \frac{\int_0^\infty C(t) \, \mathrm{d}t}{\int_0^\infty c_a(t) \, \mathrm{d}t} \tag{25}$$

where $C(t)$ is the tracer concentration with respect to a well mixed compartment and $c_a(t)$ is the tracer plasma concentration of the arterial input. However, it is not obvious that (25) is valid also for a continuous one-compartment field model where the voxels are feeding each other. We will now prove that (25) is nevertheless valid.

Let us consider the recursive expression (18) for the contrast agent concentration. Following [1] we first remark that it holds for $J_i(s) := 1/\phi_i \cdot I_i(s)$ and the special case $J_i(s) := P_i/\phi_i \exp(P_i/\phi_i s)$ that $\int_{-\infty}^\infty J_i(s) \, \mathrm{d}s = 1$. This relationship allows us to estimate the integral over $J_i * c_\mathrm{a}$ using Fubini's Theorem as follows:

$$\int_0^\infty (J_i * c_\mathrm{a})(s) \, \mathrm{d}s = \int_0^\infty c_\mathrm{a}(s) \, \mathrm{d}s. \tag{26}$$

Combining this result recursively with (18) yields:

$$\int_0^\infty C_i(s) \, \mathrm{d}s = \phi_i \int_0^\infty c_\mathrm{a}(s) \, \mathrm{d}s \tag{27}$$

and hence (25) follows.

IV. Numerical Implementation

Based on the field models described in Section III, we now establish an experimental setup suited to study the performance of the traditional methods in a synthetic flow field with a known ground truth. Using (9) and (13) we set up a forward simulation of blood flow and indicator dilution through the capillary system. We aimed at creating a generic synthetic test case and kept all optional parameters as simple as possible.

A standard arterial input function was chosen [10], the gamma-variate function $c_{\mathrm{a}}(t) := D_0(t-t_0)^{\alpha}e^{-(t-t_0)/\beta}$ for default parameters $\alpha = 3$, $D_0 = 1$, $\beta = 1.5\,\mathrm{s}$ and $t_0 = 0\,\mathrm{s}$. Ground truth perfusion was chosen as 50 ml/min/100ml, within the average range reported for brain perfusion [19], [20]. The field of view was chosen as $3\,\mathrm{mm}\times 3\,\mathrm{mm}\times 1\,\mathrm{mm}$, being within the same order as the characteristic length of the capillary bed or individual capillaries, ranging from 0.1 mm to 3 mm [14], or 0.25 mm to 850 mm [21]. The source term was assigned to the upper left voxel and the sink term was assigned to the lower right voxel. The source can be understood as the arterial compartment, the sink as the venous compartment, and the remaining field of view as the capillary system. Permeability was chosen to be isotropic and constant throughout the domain $\mathbf{k} = k\mathbf{I}$ for the identity $\mathbf{I}$ and $k = 5\times 10^{-6}\,\mathrm{mm}^2$. Dynamic blood viscosity was chosen as $\mu = 5\times 10^{-6}\,\mathrm{kPas}$ according to [22]. Porosity (e.g. CBV) was assumed to be $\phi = 0.05$, in line with measured CBV of the brain [20]. A voxel size of $0.05\,\mathrm{mm}\times 0.05\,\mathrm{mm}\times 1\,\mathrm{mm}$ was applied for the PDE model, but later relaxed when reconstructing perfusion by the traditional methods. From the porous media model using (9) and (13), streamlines were found from tracking of the flux vector field q by FACT [23], known from tractography within diffusion tensor imaging (DTI). The flow field obtained by the PDE model is visualized in Figure 3 (a).

Equation (9) was solved numerically using two-point flux-approximation, well known within porous media simulations [24]. The transport of CA described in (12) was implemented using first order upwinding [25], yielding a discrete 2D+time CA concentration map $C(x_i, t_j)$.

V. Results

A. Reconstruction of perfusion within synthetic data

We tested the convolution based traditional model (bSVD) (3) as well as maximum-slope (MS) model (5) for their capability to recover perfusion. Prior to reconstruction, the CA concentration map $C(x_i, t_j)$ was downsampled to a time-resolution of $0.1\,\mathrm{s}$. In order to simulate different spatial resolutions of the scanning process, the data was averaged using different block-sizes ranging from $(1,1)$ pixel (i.e. same resolution as the PDE model) to $(64, 64)$ pixels (i.e. entire domain). Success of restoration was measured in terms of averaged relative error of the recovered perfusion with respect to the ground truth perfusion, $RE := |P_{\mathrm{rec}} - P_{\mathrm{true}}|/P_{\mathrm{true}} \cdot 100\%$. The recovered perfusion was compared against the two perfusion maps P_{v} and P_{s} depicted in Figure 3.

The local perfusion map P_{v} was set up according to (15). Since normalization is performed with respect to voxel size, the values are unrealistically high and will vary with the discretization. As (17) shows, this can nevertheless be regarded a valid definition of perfusion since it models the feeding of arterial blood to a control region.

The global perfusion map P_{s} was set up using the definition along the streamlines (24). This definition most accurately reflects the physical perfusion at a given location and shows plausible perfusion values, cf. Figure 3. However, we do not expect the traditional models to be able to recover these values either. To quantify the errors occurring by traditional methods, the global arterial input function was used for the deconvolution, as measured in the source.

Results from deconvolution by traditional methods are displayed in Table I. For the complete domain (i.e. block size 64×64), both the MS method as well as the convolution method were able to restore the ground truth perfusion of 50 ml/min/100ml accurately with errors of $< 1\%$ and 4% respectively. However, the errors are increasing as methods are applied to smaller blocks of the system. If compared to P_{v}, one can see that results are clearly improving with increasing block size. Note that the block size of $(0.5, 0.5)$mm is within the range of resolution available on clinical scanners today, and is therefore clinically interesting. Also a clear advantage of the bSVD method as compared to MS can be observed for larger block sizes.

Results from reconstructing the porosity ϕ (i.e. CBV) according to (25) are also shown in Table I. The errors are low, independent of block size.

Table I

Median, relative error RE (%) of reconstructed perfusion compared to the ground truth values P_{v}, P_{s} and CBV from the digital phantom. Both reconstruction models MS and bSVD are able to restore the perfusion for the entire domain, but fail when dividing the domain into smaller block sizes. For larger block sizes the bSVD model restores the perfusion more accurately than the MS model. However, the blood volume ϕ is recovered accurately, independent of block size. P_{s} is only defined within a coupled system having streamlines and can therefore not be compared with restored perfusion for the entire domain.

	P_{v}		CBV	P_{s}	
block size (mm)	bSVD	MS		bSVD	MS
(0.05,0.05)	93%	98%	<1%	423%	95%
(0.23,0.23)	67%	90%	<1%	387%	90%
(0.5,0.5)	44%	79%	<1%	292%	82%
entire domain	4%	<1%	<1%		

B. Reconstruction of perfusion within real data

Experimental results from Section V-A indicate that application of the deconvolution model to patches of tissues would lead to over estimation of blood flow as compared to the overall flow within the volume of interest. In order to illustrate that this effect also may be observed on a complete dataset, we applied the deconvolution model to a clinically acquired human perfusion CT dataset of a 56 years old male male admitted with suspicion of stroke to the Radboud University Medical Center in Nijmegen, the Netherlands. The perfusion scan was obtained using a Toshiba Aquilon ONE scanner, pixel-size $0.43\,\mathrm{mm}\times 0.43\,\mathrm{mm}$, slice thickness $0.5\,\mathrm{mm}$, contrast agent $50\,\mathrm{mL}$ Xentix 300, total scan-time $114\,\mathrm{s}$, time

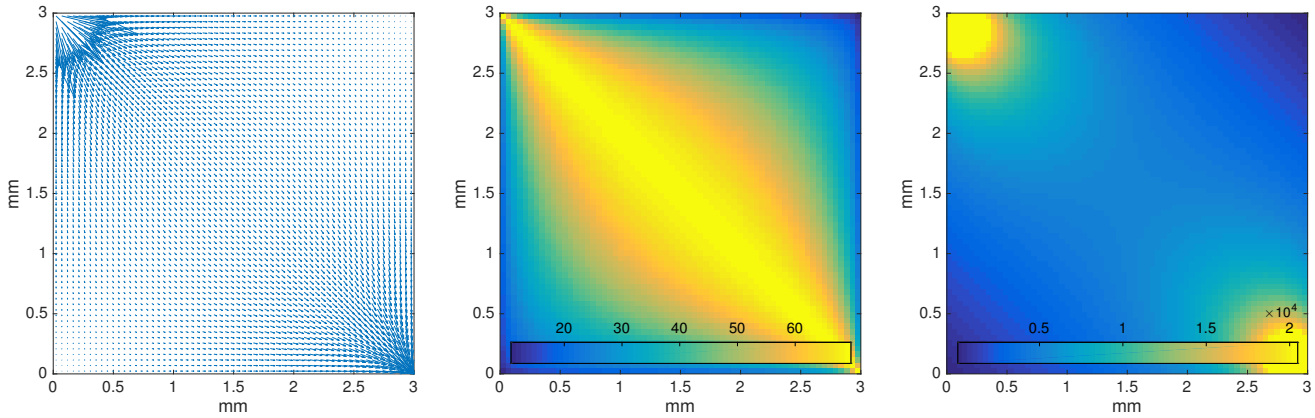

(a) Synthetic flow field $q(x)$ (b) Perfusion P_{s} along the streamlines (c) Local perfusion P_{v}.

Figure 3. Porous media (PM) flow model with a source in the upper left corner and a sink in the lower right corner. (a) Flow field by the PDE model used to simulate distribution of the contrast agent. (b) Perfusion along the streamlines according to (24). (c) Local perfusion according to (15).

resolution ranging from $2.1\,\mathrm{s}$ in the early- to $30\,\mathrm{s}$ in the late phase of CA uptake. The arterial input function was manually selected by a medical expert within the middle cerebral artery (MCA). Since we expected to see local over estimation effects mainly for small voxel sizes, the data was processed at full resolution ($512\times512\times320$) voxels. However, in order to deal with noise it was necessary to apply a prior gaussian smoothing with standard deviation of 1 voxel. Relative concentrations were estimated from the CT signal assuming a spatially independent proportionality constant. The brain tissue was segmented automatically and used as ROI for the perfusion analysis. CBF was then estimated voxel wise using a Matlab implementation of bSVD, yielding an average CBF of $64.357\,\mathrm{ml/min/100ml}$. Furthermore, we estimated the perfusion for the whole volume of interest by averaging the concentration values first and then performing the bSVD, yielding a total CBF of $24.791\,\mathrm{ml/min/100ml}$. Voxel wise results are depicted in Figure V-B.

VI. Discussion

In this work we have studied the impact of traditional 1C models to perfusion reconstruction in a coupled system of blood flow in the capillary system. To establish ground truth values, we developed a PDE based digital phantom to simulate blood flow as porous media flow within a slab of capillary tissue. We have shown that the discretized PDE problem can be equivalently described as a system of coupled traditional one-compartment models.

Our results strongly support the usage of traditional models for entire regions which are exclusively fed by the measured arterial input. However, they also show that if traditional models are applied only to parts of the system, they tend to overestimate the actual perfusion. The reason for this is that traditional models do not take into account the correct distribution volume and therefore become discretization dependent. Note that taking local arterial input functions is no remedy for this problem, since the resulting perfusion will depend heavily on the voxel size and overestimate the actual flow, cf. Figure 2 and (17). In fact, in the most extreme example we measured overestimated perfusion values of up to 423%. The results from the digital phantom are supported by real-data experiments, where we showed local overestimation of perfusion for small voxel-sizes as compared to an averaging of concentrations for the entire volume of interest. Regarding the CBV estimates, one can observe from Table I that estimation of blood volume is far more stable, and even various block sizes had little impact on the results. These results are in well agreement with the analytical considerations in Section III-E, stating that (25) is valid for entire organs as well as for single voxels. Thus, these results support the usage of (25) for computing the CBV with high accuracy for any type of block size, including single voxels.

Furthermore we have introduced two definitions of voxel wise perfusion. The perfusion P_{s} models perfusion along the streamlines and most accurately reflects the physical notion of volume flow within the correct distribution volume according to mathematical definitions. We showed that P_{s} is a global quantity along the streamline, but scales with streamline length and geometry. Theory and experiments show that the traditional models cannot recover this perfusion. The usage of P_{s} in reconstructing perfusion might as well be challenging as the entire geometry and microscopical flow patterns would have to be known to track the streamlines. However, for our purpose P_{s} was useful to clarify the concept of perfusion as a flow that must be normalized along its entire capillary length, when the blood undergoes a transition from arterial to venous blood. For future developments of field models, multi compartment models as suggested in [8] might be more applicable, where the perfusion was suggested as the non-zero divergence of the arterial flux.

Perfusion P_{v} was set up based on the interpretation of a coupled system between adjacent voxels. Theory and examples show that this definition of perfusion does not comply with the physical understanding of perfusion since it depends heavily on the discretization. However, we have shown that traditional models would restore this local value if the correct (local) arterial input function was selected. We have additionally analyzed, both analytically and experimentally, the impact of selecting a further upstream arterial input function. Specifically, we have provided an analytic expression for the

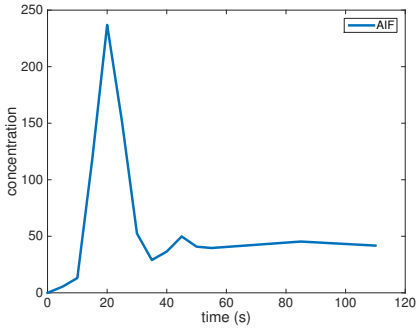

(a) Arterial input function

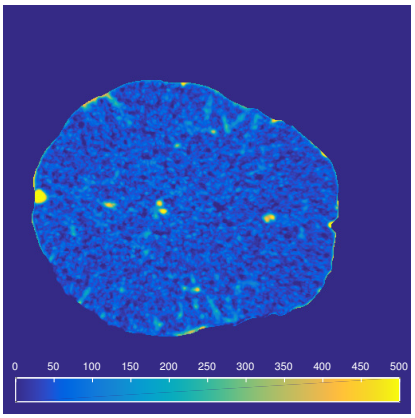

(b) One slice of the voxel-wise CBF reconstruction.

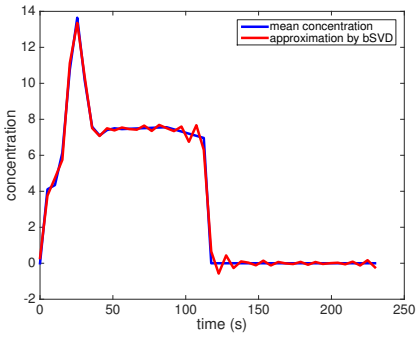

(c) Mean CA concentration curve of the whole volume of interest for reconstruction.

Figure 4. Results from real-data experiments (see Sec. V-B for details on the data). (a) AIF manually selected from the MCA. (b) One slice of the voxel-wise CBF-reconstruction for a 3D volume of interest. (c) Mean concentration curve for the complete 3D volume of interest and the curve approximation by bSVD.

impulse response function which shows that the perfusion will depend on the flow at all upstream voxels, and that the traditional convolution method finds the recursive impulse response function for all upstream voxels according to (19). However, the drawback of this approach is that the correct distribution volume is not accounted for and the obtained perfusion values will be overestimated.

VII. Conclusion

In conclusion, our experiments show that if traditional methods for perfusion estimation are applied to a coupled system they perform well if applied to the entire domain, but tend to fail when applied only parts of the system. We have illustrated this effect in detail in the case of high resolution images where the voxel size reaches the spatial dimension of the capillary systems, but also showed the effect on coarse scale real data.

The reason for this failure is not numerical instabilities in the deconvolution, but rather that perfusion becomes overestimated since the traditional models will not account for the correct distribution volume.

This problem is expected to become more pronounced in future as imaging hardware is constantly improving in spatial resolution. We expect to find overestimation also in pathological tissue, where fluid is passing through multiple, adjacent voxels, and recommend to be take this effect into consideration in clinical evaluation of the data. To account for this problem, the development of new field models for perfusion is therefore highly demanded, in line with approaches described in [8], [16].

References

[1] S. Sourbron and D. Buckley, "Classic models for dynamic contrast-enhanced MRI," *NMR Biomed*, vol. 26, no. 8, pp. 1004–1027, 2013.

[2] Q. Feng *et al.*, "Voxel-level comparison of arterial spin-labeled perfusion magnetic resonance imaging in adolescents with internet gaming addiction," *Behav Brain Funct*, vol. 9, no. 1, p. 33, 2013.

[3] Y. Chen *et al.*, "Voxel-level comparison of arterial spin-labeled perfusion mri and fdg-pet in alzheimer disease," *Neurology*, vol. 77, no. 22, pp. 1977–1985, 2011.

[4] K. Kudo *et al.*, "Differences in CT perfusion maps generated by different commercial software: Quantitative analysis by using identical source data of acute stroke patients 1," *Radiology*, vol. 254, no. 1, pp. 200–209, 2010.

[5] K. Zierler, "Indicator dilution methods for measuring blood flow, volume, and other properties of biological systems: a brief history and memoir," *Ann Biomed Eng*, vol. 28, no. 8, pp. 836–848, 2000.

[6] F. Calamante, P. Yim, and J. Cebral, "Estimation of bolus dispersion effects in perfusion MRI using image-based computational fluid dynamics," *Neuroimage*, vol. 19, no. 2, pp. 341–353, 2003.

[7] R. M. Henkelman, "Does ivim measure classical perfusion?" *Magnetic resonance in medicine*, vol. 16, no. 3, pp. 470–475, 1990.

[8] S. Sourbron, "A tracer-kinetic field theory for medical imaging," *IEEE Trans Med Imaging*, 2014.

[9] H. Darcy, "Les fontaines publiques de la ville de dijon," *Victor Dalmont*, p. 647, 1856.

[10] L. Østergaard *et al.*, "High resolution measurement of cerebral blood flow using intravascular tracer bolus passages. part i: Mathematical approach and statistical analysis," *Magn Reson Med*, vol. 36, no. 5, pp. 715–725, 1996.

[11] T. Boutelier *et al.*, "Bayesian hemodynamic parameter estimation by bolus tracking perfusion weighted imaging," *IEEE T Med Imaging*, vol. 31, no. 7, pp. 1381–1395, 2012.

[12] O. Wu *et al.*, "Tracer arrival timing-insensitive technique for estimating flow in mr perfusion-weighted imaging using singular value decomposition with a block-circulant deconvolution matrix," *Magn Reson Med*, vol. 50, no. 1, pp. 164–174, 2003.

[13] E. Klotz and M. König, "Perfusion measurements of the brain: using dynamic CT for the quantitative assessment of cerebral ischemia in acute stroke," *Eur J Radiol*, vol. 30, no. 3, pp. 170–184, 1999.

[14] Y.-I. Cho and D. J. Cho, "Hemorheology and microvascular disorders," *Korean Circ J*, vol. 41, no. 6, pp. 287–295, 2011.

[15] A. Cookson *et al.*, "A novel porous mechanical framework for modelling the interaction between coronary perfusion and myocardial mechanics," *J Biomech*, vol. 45, no. 5, pp. 850–855, 2012.

[16] C. Michler *et al.*, "A computationally efficient framework for the simulation of cardiac perfusion using a multi-compartment darcy porous-media flow model," *Int J Numer Method Biomed Eng*, vol. 29, no. 2, pp. 217–232, 2013.

[17] L. Evans, *Partial differential equations*, 2nd ed. Providence, Rhode Island: American Mathematical Society, 1998.

[18] W. Kordecki, "Reliability bounds for multistage structures with independent components," *Stat Probabil Lett*, vol. 34, no. 1, pp. 43–51, 1997.

[19] W. D. Obrist *et al.*, "Cerebral blood flow and metabolism in comatose patients with acute head injury: relationship to intracranial hypertension," *J Neurosurg*, vol. 61, no. 2, pp. 241–253, 1984.

[20] A. Smith *et al.*, "Whole brain quantitative CBF, CBV, and MTT measurements using MRI bolus tracking: Implementation and application to data acquired from hyperacute stroke patients," *J Magn Reson Imaging*, vol. 12, no. 3, pp. 400–410, 2000.

[21] M. I. Townsley, "Structure and composition of pulmonary arteries, capillaries, and veins," *Compr Physiol*, 2012.
[22] R. Rosencranz and S. Bogen, "Clinical laboratory measurement of serum, plasma, and blood viscosity," *Am J Clin Pathol*, vol. 125 Suppl, pp. 78–86, Jun 2006.
[23] S. Mori, B. Crain, and P. van Zijl, "3D brain fiber reconstruction from diffusion MRI," in *Proceedings of International Conference on Functional Mapping of the Human Brain*, 1998.
[24] J. Aarnes, T. Gimse, and K.-A. Lie, *An introduction to the numerics of flow in porous media using Matlab*. Springer Verlag, 2007.
[25] S. Patankar, *Numerical Heat Transfer and Fluid Flow*, 1st ed. Hemishpere Publishing Corporation, 1980.